Utilization of Titanium- and Indium-based Metal-Organic Frameworks for Dye Sensitized Solar Cells

A Thesis Report

Presented to

The Faculty of the Department of Chemistry and Biochemistry

California State University Los Angeles

In Partial Fulfillment

of the requirements for graduation from the

Chemistry and Biochemistry Department Honors Program

By

Tommy Taing

May 2025

ABSTRACT

Utilization of Titanium- and Indium-based Metal-Organic Frameworks for Dye Sensitized Solar Cells

Tommy Taing

This study investigates the impact of three metal-organic frameworks (MOFS) on the performance of solid-state dye-sensitized solar cells (ssDSSCs). Three MOFs were examined: two synthesized using titanium ($Ti_6O_6(OiPr)_6(abz)_6$) and indium ($In(NO_3)_3 \cdot H_2O$) clusters in combination with the ligand tetrakis(4-carboxyphenyl)porphyrin. The MOFs were employed as photosensitizing dye to evaluate their influence on solid-state dye-sensitized solar cell (ssDSSC) performance. The third MOF was synthesized by doping the indium-based framework (In-TCPP) with tin, resulting in In-TCPP(Sn). Solar cells were fabricated on fluorine doped tin oxide (FTO) glass substrates coated with titanium oxide nanoparticles, anchor, MOF dye, hole-transporting material, and gold layers. The crystallinity of the MOFs was analyzed using powder X-ray diffraction (PXRD), optical properties were assessed using UV–Visible spectroscopy, and electrochemical behavior analyzed with cyclic voltammetry. The current density vs voltage curves of the solar cells were generated through linear sweep voltammetry. The doped In-TCPP(Sn) demonstrated the highest power conversion efficiency (PCE, η) of 0.0242%. In-TCPP had a PCE of 0.0119% and Ti-TCPP had $2.23e^{-5}$%. Electron lifetime measurements confirmed photoinduced electron injection into the TiO_2 layer, as evidenced by a reduction in electron lifetime relative to the open-circuit voltage.

ACKNOWLEDGMENTS

I would like to thank Dr. Yangyang Liu, my principal investigator and thesis advisor. From the moment I first discovered and asked to join her lab to the current day, she has helped cultivate my skills as a researcher. Additionally, her push for me to adopt more responsibilities in the lab and exposure to researching opportunities has helped me immensely. I am forever thankful she decided to allow me into her lab. I would also like to thank my committee members Dr. Dianlu Jiang and Dr. Petr Vozka for their support throughout this process alongside their support of me as a researcher.

I also give many thanks to the other members of the lab, who have supported my journey throughout my stay here. Their support has been instrumental in helping me develop my skills quickly and become familiar with the rigors of research. I would especially like to thank my mentor, Jesus Corona, and Matthew Tang. Both have been amazing role models and have spent much time helping me learn or clarify topics that I did not fully grasp. Their support has greatly expedited the project's timeline. Additionally, I thank Dorotheo Manriquez for aiding me in the research process and providing helpful resources. I am glad I became a member of this lab.

Additionally, the support of my family has been instrumental to allowing this project to come to fruition. They have been avid supporters, helping me stay motivated in pushing through the work.

This research was funded by the NSF CREST program, the Center for Advancement toward Sustainable Urban Systems or CATSUS (HRD-2112554). This work also acknowledges support from the U.S. Department of Energy, Office of Science, Office of Basic Energy Sciences, under the Award Number DE-SC0024498.

TABLE OF CONTENTS

LIST OF TABLES

Table

LIST OF FIGURES

Figure

Introduction

Section 1.1 – Solar Cells

The impact of climate change is evident, with the extensive reliance on fossil fuels—such as coal, natural gas, and petroleum—releasing a wide range of greenhouse gases (methane, nitrogen oxides, and carbon oxides) that have significantly contributed to agricultural damage, air pollution, and disruptions in global climate patterns.[1,2] Solar energy has garnered considerable attention, prompting research into effective methods for harvesting and utilizing sunlight for electricity generation.[1,3] One of the most common methods of solar energy capture uses photovoltaic technology, which is the conversion of light to electricity in the form of solar cells. Researchers have explored a variety of solar cells, such as silicon-based, thin-film, perovskite, organic, and dye-sensitized solar cells (DSSCs).[4] Among these technologies, DSSCs have attracted significant interest due to their low fabrication costs, compatibility with roll-to-roll manufacturing, and potential for high power conversion efficiencies (η) under both high-intensity and diffuse lighting conditions. DSSCs that utilize a solid-state dye material and a hole-transporting material (HTM) are called solid-state dye-sensitized solar cells (ssDSSCs), and they are especially attractive as they avoid the usage of liquid electrolytes that may leak or evaporate under extreme weather conditions.[5,6]

DSSCs, or Grätzel cells, are a type of cost-efficient, environmentally friendly solar cell that typically feature a working electrode, a counter electrode, a transparent conducting oxide (TCO) coated glass substrate, and an electrolyte or photosensitive dye in solid state devices.[6–8] The working electrode, or photoanode, consists of a wide-bandgap semiconducting material, typically n-type TiO_2, alongside a molecular dye that

is deposited on TCO in a uniform nanocrystalline arrangement. Owing to its stability, nontoxicity, and low cost, TiO_2 is one of the most common semiconductor materials. However, its large bandgap of 3.2 eV necessitates either doping of the nanocrystals or the use of a molecular dye to improve absorption of direct and diffuse light.[9,10] The counter electrode consists of a layer of an inert but highly conductive metal, which is typically gold or platinum. The photosensitive molecular dye harvests photons from light and generates excited electrons, injecting them into the TiO_2. When the electron is excited, a hole or vacancy is left behind in the molecular dye. A redox mediator, such as a hole-transporting material (HTM), supplies an electron to regenerate the dye, allowing the excitation cycle to continue. The HTM is regenerated through the charge transfer of the excited electron at the counter electrode, completing the cycle. A schematic of the cell fabrication process and the electron flow is depicted in Figure 1. While the process is capable of power conversion, the DSSC is prone to efficiency loss through high electron recombination rates and nanoscale agglomeration formation, disrupting the electron transfer process. Therefore, the development of materials that can mitigate these limitations is critical for enhancing power conversion efficiency.

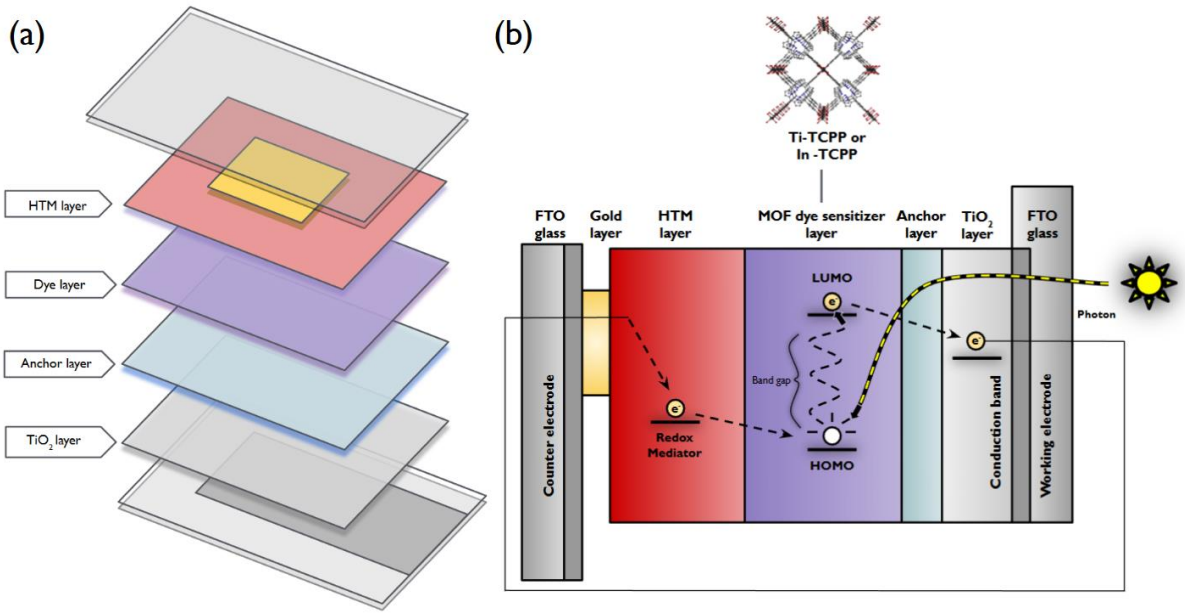

Figure 1. Schematic of DSSCs and electron flow. (a) Assembly of DSSC layers. (b) schematic of the electron flow in DSSCs.

Section 1.2 – Metal-Organic Frameworks Application in ssDSSCs

Metal–organic frameworks (MOFs) are porous structures composed of metal nodes coordinated to organic ligands. These components form strong coordinate covalent bonds, resulting in crystalline frameworks that exhibit high surface area, chemical resilience, and thermal stability. In addition, the inherent tunability of MOFs enables the design of light-absorbing structures with redox activity. Recent research has focused on utilizing MOFs as photocurrent-enhancing materials in dye-sensitized solar cells (DSSCs) due to their potential as solid-state photosensitizers.[11–13] A large subset of MOFs are porphyrin-based structures, which have garnered interest due to its photovoltaic capabilities. The expansive π-conjugation of the porphyrin ligand and characteristic Soret and Q bands at the narrow blue region of 400-450 nm and red region

of 500-700 nm, respectively.[14] However, while the porphyrins have a narrow bandwidth, modification through MOF synthesis offers the potential for enhancing electron transfer and expanding the light absorption range.[15,16] Moreover, MOFs retain chemical and thermal stability when utilizing porphyrin-based linkers, allowing their utilization under various conditions. While efforts have been directed to explore the application of porphyrin MOFs on ssDSSCs, the analysis of the porphyrin MOFs on power conversion efficiency and the effects of dopants are underexplored.[1,11,14,17]

To address this gap, we have assembled solid-state DSSCs utilizing titanium- and indium-based porphyrin MOFs. These MOFs had metal nodes linked together with the ligand tetrakis(4-carboxyphenyl)porphyrin (TCPP). The titanium cluster ($Ti_6O_6(OiPr)_6(abz)_6$) acted as the metal node and, with TCPP as the ligand, the MOF Ti-TCPP was synthesized. In-TCPP followed a similar synthesis, with the indium cluster ($In(NO_3)_3 \cdot H_2O$) acting as the metal node. Additionally, a tin dopant was incorporated into the porphyrin to create In-TCPP(Sn), and all three MOFs effect on the solar cell performance were analyzed. Due to its large system of conjugated π-electrons and tunable structure, TCPP offers viability as an efficient charge stabilization of an excited electron and charge injection into the conduction band of the semiconductor.[18] The strong absorption bands characteristic of porphyrins, (Soret and Q bands), allow for the possibility of expanding the absorbed light range of the TiO_2 (200-400 nm) and capturing a larger portion of the visible and near-infrared (NIR) region solar radiation.[10,19,20] The synthesized Ti-TCPP, In-TCPP, and In-TCPP(Sn) MOFs would act as the photosensitizer within the dye layer of the solar cell, allowing for electron capture and potential for improving charge injection. The thin MOF dye films would be drop cast and, using

benzene-1,4-dicarboxylic acid (BDC) as an anchoring group between the dye and TiO_2, coordinated to the TiO_2 deposited on the surface of the transparent fluorine doped tin oxide (FTO) glass substrate. The power conversion efficiency of light to energy from the photovoltaic MOFs when implemented as the dye layer in the DSSCs was studied.

Experimental Methods

Section 2.1 - Preparation of Etching Solution and Titanium Dioxide Nanoparticles

A 2 M HCl etching solution was prepared. Titanium dioxide (TiO_2) compact layer was prepared by mixing isopropanol (6 mL), titanium-n-butoxide (0.9 mL), and ethanolamine (0.19 mL) in a microwave vial, and continuously stirred at 40°C for 2 h. The vial was stored in a refrigerator at 4°C. The nanocrystalline titanium colloid layer was prepared by mixing titanium (IV) n-butoxide (12.5 mL) with isopropanol (4 mL), with 0.1 M HNO_3 (150 mL) added drop wise to the solution under continuous stirring. After hydrolysis, the slurry is stirred at 80°C for 8 h and then autoclaved at 200°C for 12 h.

The 0.01 M anchor benzene-1,4-dicarboxylic acid (BDC) solution was prepared by mixing terephthalic acid (166 mg) and KOH (112 mg) in anhydrous ethanol (100 mL) and constantly stirred at 70°C for 4 h.

Section 2.2 - Preparation of Hole Transporting Material and Titanium Cluster

The hole transporting material (HTM) was prepared in the glovebox by mixing Spiro-MeOTAD (72.3 mg), lithium bis(trifluoro) methane sulfonic acid (10 mg), Co(III) TFSI salt (10 mg), chlorobenzene (1 mL), and tert-butyl pyridine (27 µL) in a vessel wrapped with tinfoil. The solution was sonicated for 20 mins and left in the glovebox for storage.

The titanium cluster ($Ti_6O_6(OiPr)_6(abz)_6$) was synthesized by adding $Ti(O\textit{i}Pr)_4$ (7.5 mmol, 1.97 mL) dropwise to a solution made up of isopropanol (2.75 mL), $Mn(NO_3)_2$ (1 mmol, 293.03 mg), and 3,3-Dimethylbutyric acid (7.5 mmol, 0.79 mL) under continuous

stirring at 80ºC for 24 h. The white crystal product was washed with isopropyl alcohol and acetone. The product was dried at 60ºC in a vacuum oven for 8 h.

Section 2.3 - Preparation of Ti-TCPP, In-TCPP, and In-TCPP(Sn)

Ti-TCPP was synthesized by mixing the titanium cluster ($Ti_6O_6(OiPr)_6(abz)_6$) (4 mg), TCPP (15 mg), benzoic acid (200 mg), and DMF (3 mL) in a 15 mL pressure vessel. The dissolved contents were placed in an oven at 150°C for 48 h and washed with DMF (5 mL) and acetone (5 mL) 3 times respectively for each solvent. The contents were dried under vacuum at 60°C for 8 h and dark red crystals were harvested.

The In-TCPP ($[In_2(H_2TCPP(OH)_2]\cdot 3DMF\cdot 4H_2O$) was synthesized by adding 0.5 M aqueous $In(NO_3)_3\cdot H_2O$ (75.6 μL), DMF (724 μL), and TCPP (15 mg) into a 15 mL pressure vessel, heated for 48 h at 120°C, and washed with DMF (5 mL) and acetone (5 mL) 3 times, respectively. The washing cycle would yield purple In-TCPP crystals for harvesting.

The dichlorido-5,10,15,20-tetrakis(*p*-carboxyphenyl)-porphyrinato-tin(iv), or TCPP(Sn), was synthesized by taking a solution of TCPP (1.29 g, 1.63 mmol) in pyridine (50 mL) and mixing the solid $SnCl_2\cdot 2H_2O$ (730 mg, 3.25 mmol). The solution was refluxed in the dark for 2 h and diethylether (250 mL) was added to the cold solution. After being left in the dark for 12 h, the precipitate was washed with ether (20 mL), CH_2Cl_2 (20 mL), DI water (20 mL) and ether (20 mL) 4 times respectively for each solvent. The In-TCPP(Sn) was fabricated using the same process for the In-TCPP by replacing the TCPP with the TCPP(Sn) linker.

Section 2.4 - Fabrication of Solar Cells

The dye-sensitized solar cells were fabricated through a multi-step process. The FTO glass, which was 1.5 x 2 cm, utilized polyimide tape to preserve a portion of the conductive face. The tape was aligned with the 1.5 cm bottom edge of the cell. The tape was cut ¼ cm on both sides of the cell to expose the conductive face and a ½ cm portion cut parallel to the top edge of the cell to yield a smaller rectangle covering much of the glass face.

The taped cells were etched using HCl by submerging the surface of the taped cells for 1 min. The solution was neutralized using zinc powder on the surface of the cells and addition of potassium carbonate alongside water to a pH of 8. The tape was removed after neutralization and the cells washed with 1% micro-soap solution, isopropanol, acetone, and distilled water through sonication. The washed cells had the surface plasma cleaned for 20 min.

The cleaned cells had ¼ cm polyimide tape attached across the bottom edge and placed inside a spin coater within the glovebox. The cells had 0.3 mL of compact TiO_2 deposited dropwise at the center. The cells were removed from the glovebox and, peeling off the tape, placed in a furnace at 500°C for 10 h. The titanium colloid nanoparticles were deposited onto the cell surface by retaping the cell in the same fashion, heating the cells to 100°C, and quickly dropwise depositing the colloid onto the surface of the cell using the spin coater. The tape was removed and cells placed in a furnace at 500°C for 10 h. The cells were taken from the oven, retaped the same way, and placed into vials with their conductive face upwards.

The conductive face was submerged under the anchor solution and left for 24 h at 60°C to ensure layer settlement. The anchor-soaked cells were taken out where 0.1 M suspension solutions of the prepared MOFs (Ti-TCPP, In-TCPP, and In-TCPP(Sn)) were drop-casted at 60, 90, 120, 150, and 180 μL. The drop cast followed 30 μL depositions, with 10 min intervals between each deposition. The cells were brought into the glovebox and placed onto the spin coater where HTM (50 μL) was deposited dropwise onto the cells. Avoiding light exposure, the cells were taken out of the glovebox and the cell was taped to preserve a square (0.5 cm x 0.5 cm) center. The cells were placed in the chamber of the gold sputter to generate a uniform gold layer on the cell.

The gold layered cell was electrochemically analyzed by overlapping the conductive side of a blank cell on top of the layered gold side of the complete cell. The reference and counter electrodes were attached to the blank cell and the working electrode to the layered cell. Light shone through the back of the layered cell to determine the efficiency of the cell. The data was processed and the plots of the open circuit voltage vs the short circuit density were generated.

Section 2.5 - Characterization and Instrumentation

The UV-vis spectroscopy was done using a UV-vis spectrophotometer (Shimadzu) with an integrating sphere accessory. An auto-Lab spin coater was utilized and set to 2000 rpm. Liquid samples were analyzed using an NMR machine (Bruker). Powder X-ray diffraction spectra were generated using an X-ray diffractometer (Bruker). The plasma cleaner utilized a vacuum pump and vacuum closing chamber. A gold sputter coater was utilized with argon gas at 5 psi. Electrochemical data was gathered using a CHI 610 model electrochemical analyzer, and the current vs potential response graph analyzed using linear

sweep voltammetry technique. Additionally, the model electrochemical analyzer was utilized for the cyclic voltammetry measurements.

Results and Discussion

Section 3.1 – Characterization of Ti-TCPP, In-TCPP, and In-TCPP(Sn) MOFs

The solvothermal synthesis of Ti-TCPP and In-TCPP MOFs yielded brownish red and purple powders, respectively. The In-TCPP(Sn) and the TCPP(Sn) ligand were green powders, which could be attributed to an absorbance change resulting from the upshift of the G-a_{2u} derived molecular orbital.[16] Additionally, TCPP has been widely studied in literature to feature imine-type pyrrole nitrogen that can bind to protons and cause the free-base porphyrin and deprotonated species to differ in optical properties.[21–25] The conformational changes that resulted from the tin dopant integration in the TCPP(Sn) and the organization of the In-TCPP(Sn) MOF may further explain the color change.

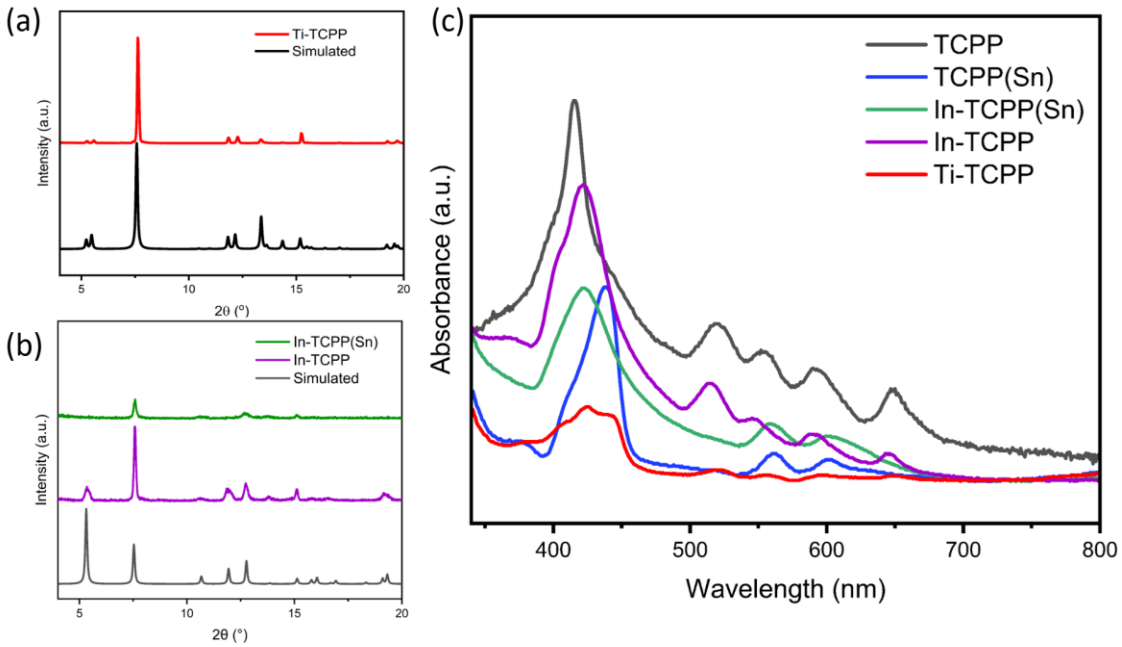

Figure 2. PXRD scans of Ti-TCPP, In-TCPP, In-TCPP(Sn), and UV-Vis of MOFs. (a) PXRD depicting the intensity vs 2θ degree change of Ti-TCPP in comparison to the simulated data. (b) In-TCPP(Sn) and In-TCPP PXRD in comparison to the simulated

data. (c) UV-Vis absorption spectra of TCPP (black), TCPP(Sn) (blue), In-TCPP(Sn) (green), In-TCPP (purple), and Ti-TCPP (red).

Using the dried MOF powders, the X-ray diffraction patterns for Ti-TCPP, In-TCPP(Sn), and In-TCPP were recorded and compared to simulated crystallography patterns. As seen in Figure 2a, Ti-TCPP had high crystallinity as evident by the clear and sharp peaks, with patterns matching well with reported simulated pattern.[26] Figure 2b compared the In-TCPP and In-TCPP(Sn) MOFs to its simulated pattern, which similarly demonstrated high crystallinity. In-TCPP had diffraction patterns that matched well with reported simulated patterns.[27] In-TCPP(Sn) matched a large majority of the simulated signals, with the loss in the signal at 5° being attributed to the integration of the tin dopant into the TCPP porphyrin center.[16] With the high crystallinity and match with the simulated patterns, the studied MOFs demonstrated successful synthesis.

The MOFs and linkers were measured and suspended in 1 M concentration solutions, which were drop cast onto the surface of FTO glass substrates for characterization testing for UV-Vis. As seen in Figure 2c, TCPP displayed the characteristic Soret band at 400-450 nm, and the Q bands seen in the 4 peaks from the range of 515-650 nm.[14,16] Ti-TCPP retained the Soret band peak at 430 nm and Q bands from 550-655 nm, with blue shifting of the Soret and Q band for both possibly resulting from the confirmational changes of the titanium cluster ($Ti_6O_6(OiPr)_6(abz)_6$) and TCPP coordination.[16,23,24] In-TCPP had the Soret band peak at 424 nm, with Q bands from 515-650 nm. The In-TCPP signals had a high match with TCPP, which could be attributed to the indium cluster's coordination with TCPP having minimal effects on a red

or blue shift. The doped ligand TCPP(Sn) demonstrated the retention of the Soret band at 440 nm, and Q bands at 560 and 600 nm, respectively. Two of the Q band peaks were dampened, which was attributed to the integration of tin in the porphyrin center causing a collapse of the four visible-region ground-state absorption bands [$Q_y(1,0)$, $Q_y(0,0)$, $Q_x(1,0)$, $Q_x(0,0)$] of the free base porphyrin to two [Q(1,0), Q(0,0)].[16,28] Similarly, In-TCPP(Sn) featured the Soret band structure at 425 nm and Q bands at 560 and 600 nm, respectively. The Q bands retained the collapsed band structure seen in TCPP(Sn). The blue shift in In-TCPP(Sn)'s Soret band from the TCPP(Sn) linker by ~25 nm was attributed to the conformational changes that occurred when the indium cluster coordinated with the tin-doped porphyrin linker.[22,23,25]

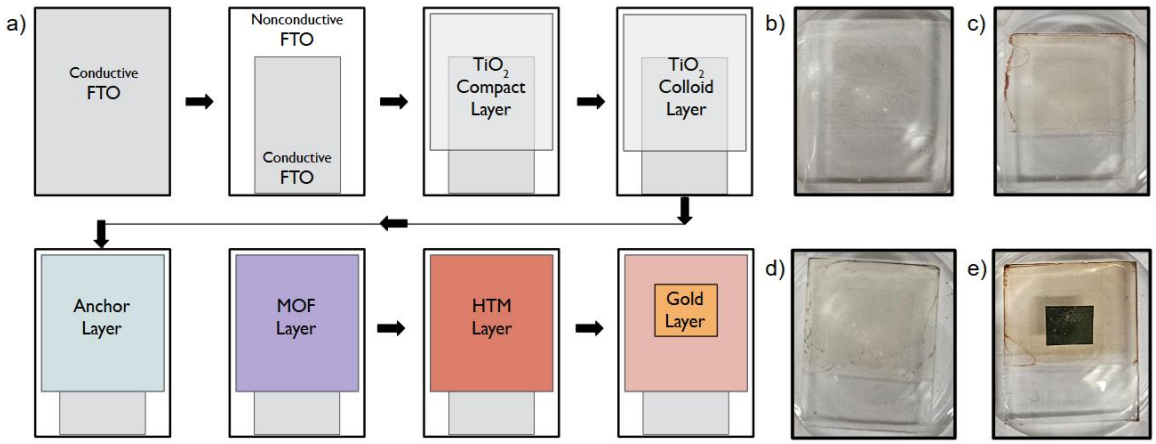

Figure 3. Schematic of DSSCs and sample cells. (a) Schematic of DSSC fabrication. Gray = conductive side of FTO glass, white = nonconductive face, light gray = titanium oxide compact and colloid nanoparticle layer, blue = anchor layer, purple = MOF layer, light purple = hole transporting material (HTM) layer, gold = sputtered gold contact. (b) Ti-TCPP cell before deposition of HTM. (c) In-TCPP cell before HTM. (d) In-TCPP(Sn)

cell before HTM. (e) Sample fabricated cell example for Ti-TCPP, In-TCPP, and In-TCPP(Sn) ssDSSCs.

Section 3.2 – Cell Fabrication

The solar cell fabrication followed the etching of the FTO glass surface to reveal a thin border of nonconductive FTO glass. The glass was spin coated with TiO_2 compact in the glovebox, heated at 500°C in a furnace, TiO_2 colloid nanoparticles spin coated onto the fresh surface, and heated at 500°C once more to anneal the particles into a thin film. The coated glass substrates are then left in a solution of 0.01 M benzene-1,4-dicarboxylic acid (BDC) for 8 h, rinsed with isopropanol, and had the prepared 0.1 M MOF or linker solution drop cast onto the surface of the cell. The hole-transporting material was then spin coated under inert air and the gold layer sputtered on to seal the layers. A simplified diagram of the process can be seen in Figure 3. The Ti-TCPP cell before HTM deposition remained highly transparent, with very little visible color on the cell surface. In-TCPP left a light purple-pink hue after depositing the MOF onto the cell surface. In-TCPP(Sn) had left a thin green film on the surface after deposition. After HTM was applied and gold sputtered on, all fabricated ssDSSCs took on a red hue with a square gold contact center.

Section 3.3 – Cell Performance and *J-V* curves

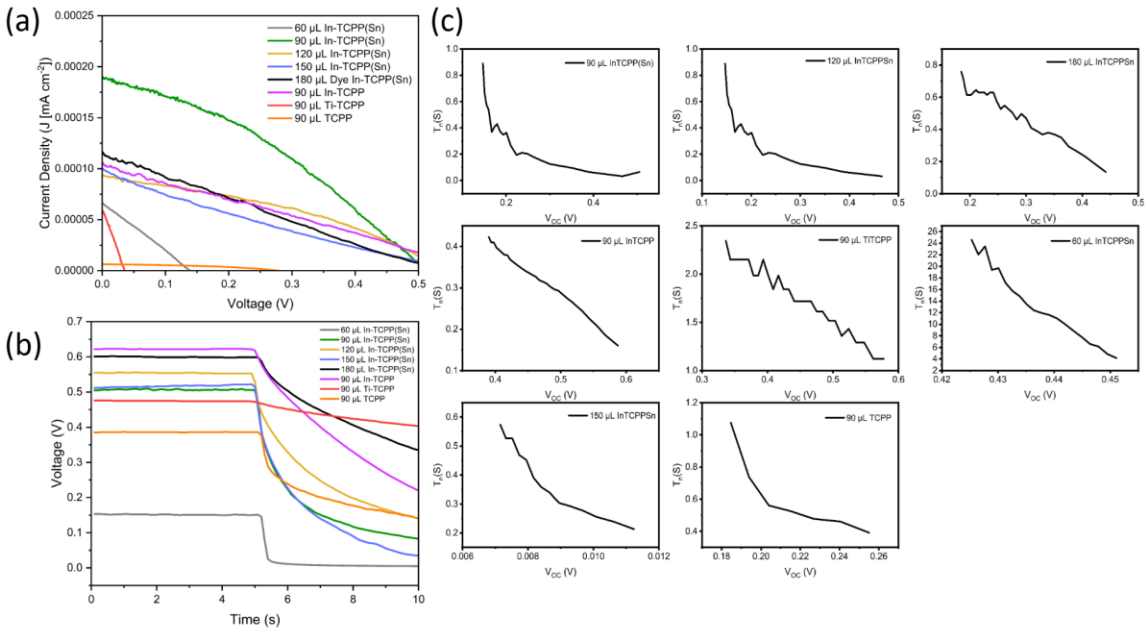

Figure 4. J-V Curves, lifetime curves and electron lifetimes. (a) *J-V* curves of solid-state dye-sensitized solar cells (ssDSSCs) based on various working electrodes. (b) Lifetime measurements of various working electrodes. (c) Electron lifetimes for each fabricated ssDSSCs.

Table 1. Characteristics of fabricated ssDSSCs performance based on various working electrodes.

MOF	Deposition Amount	V_{oc} (V)	J_{sc} (A cm^{-2})	Fill Factor (FF)	η (%)
In-TCPP(Sn)	60 μL	0.139	6.59e^{-5}	0.264	0.00177
In-TCPP(Sn)	90 μL	0.516	1.90e^{-4}	0.339	0.0243
In-TCPP(Sn)	120 μL	0.542	9.36e^{-5}	0.366	0.0135

In-TCPP(Sn)	150 μL	0.583	$1.00e^{-4}$	0.205	0.00873
In-TCPP(Sn)	180 μL	0.552	$1.16e^{-4}$	0.241	0.0112
In-TCPP	90 μL	0.5	$1.06e^{-4}$	0.309	0.0119
Ti-TCPP	90 μL	0.183	$1.01e^{-6}$	0.165	$2.23e^{-5}$
TCPP	90 μL	0.278	$7.59e^{-5}$	0.412	$6.35e^{-3}$

The characteristics of the fabricated solid-state dye-sensitized solar cells were studied, with the Ti-TCPP, In-TCPP, and In-TCPP(Sn) MOFs performance as the photovoltaic dye. In-TCPP(Sn) had cells fabricated with varying deposition amounts of 60, 90, 120, 150, and 180 μL to determine its effect on the open circuit potential (V_{oc}), the short circuit current density (J_{sc}), fill factor (FF), and power conversion efficiency (η). Figure 4a depicts the varying cell performances of In-TCPP(Sn) cells alongside the In-TCPP, Ti-TCPP, and TCPP fabrications. The efficiency of the ssDSSC under standard 'one sun' AM 1.5G illumination (100 mW cm^{-2}) can be determined through the ratio of the maximum power output, P_{max}, to the incoming light power P_{in}, which equates to the ratio of the V_{oc}, J_{sc}, and FF above P_{in} as shown in the equation below.[8]

$$\eta = \frac{P_{\max}}{P_{\text{in}}} = \frac{J_{\max} V_{\max}}{P_{\text{in}}} = \frac{J_{\text{SC}} V_{\text{OC}} \text{FF}}{P_{\text{in}}} \quad (1)$$

When comparing the effects of the deposition amount on the In-TCPP(Sn) solar cell performance, the highest performing cell from the compiled *J-V* curves was found to be using a 90 μL (~$9e^{-6}$ moles) film deposition amount, with a η value of 0.0243%. The cell had a Voc, Jsc, and FF of 0.516 V, 1.90e-4 A cm^{-2}, and 0.339, respectively. When

compared to the TCPP reference cell's values seen in Table 1, the cell had improved performance significantly. The absorbance shift caused by the coordination of the indium cluster and tin incorporation to the TCPP seems to have resulted in better charge transfer and injection into the TiO_2 layer. While the FF was lower, this was assumed to have been due to pinholes that may have formed in the dye layer from the bulkier species when coordinating with to the TiO_2 nanoparticles.[16,29,30] The lowest performing In-TCPP(Sn) cell was found to be the 60 µL (~$6e^{-6}$ moles), which had a η value of 0.00177%. The poor performance could be a result of a lower amount of MOF coordinating at the interfacing dye layer, hindering the light harvesting capability and leaving a higher number of exposed pinholes between the HTM and TiO_2 layers that acts as recombination centers.[31] When the deposition amounts were raised, the η value decreased to a low of 0.00873% as seen in the 150 µL (~$1.5e^{-5}$ moles). The decreased efficiency of the cells as the deposition amount increased could be explained by the oversaturation of MOF at the interfacial dye layer, leading to the electron charge not being transferred effectively and undergoing hole/electron recombination.[32] The increased contact surface from the dye aggregation on the surface of the TiO_2 layer could have additionally contributed to the efficiency drop due to charge trapping or pore blocking.[30] In the case of the 180 µL cell having a higher efficiency (0.0112%) than 150 µL (0.00873%), the slight increase in efficiency could be due to a larger portion of the MOF coordinating with the anchor layer to the TiO_2 layer, as the fill factor of the 180 µL (0.241) cell is higher than the 150 µL (0.205). Excluding the In-TCPP(Sn) 60 µL cell, the ssDSSCs fabricated with the MOF had higher η%, V_{oc}, and J_{sc} than the solar cell constructed with free-base TCPP as the reference photosensitizing dye.

Once the 90 μL cell performance was found to be the highest, Ti-TCPP and In-TCPP ssDSSCs were fabricated with the same deposition amount and found to have an η of 2.23e^{-5}% and 0.0119%, respectively. The Ti-TCPP cell was significantly lower than the In-TCPP and In-TCPP(Sn) solar cells, as the overall low efficiency alongside the low V_{oc} of 0.183 V demonstrated that the MOF had poor electron injection into the TiO_2.[29,30] The Jsc and FF were similarly low, with values of 1.01e^{-6} A cm^{-2} and 0.165, respectively. These low values indicate a high degree of electron trapping or poor electron injection, causing an abundance of hole/electron recombination pathways.[29] When each value was compared to its respective counterpart in TCPP, the Ti-TCPP MOF had lower values than the free-base porphyrin cell, indicating the MOF a reduced capability compared to the reference TCPP cell. For In-TCPP, the values for V_{oc}, J_{sc}, FF, and η were 0.5 V, 1.06e^{-4} A cm^{-2}, 0.309, and 0.0119%, respectively. The MOF performed better than the Ti-TCPP and the TCPP reference cell, however the recorded η was half of the In-TCPP(Sn) 90 μL cell's performance. The higher performance of the In-TCPP in comparison to the Ti-TCPP was attributed to the indium cluster having better recombination suppression, as evident by the better performance of both the In-TCPP and In-TCPP(Sn) cells.

Section 3.4 – Lifetime Evaluation and Electron Lifetimes

Figure 4b depicts the lifetimes of the fabricated Ti-TCPP, In-TCPP, and In-TCPP(Sn) cells. The lifetimes were recorded for the cells by exposing the cells to light with the lamp and, after 5 seconds, covering the light source and measuring the voltage drop. In-TCPP and In-TCPP(Sn) had rapid voltage decay, as evident by the steep slopes once illumination was cut at 5 seconds. The electron lifetime was obtained by using the

following equation, where T_e represents the electron lifetime, Boltzmann's constant k_B, temperature *T*, and elementary charge *e*.

$$\tau_n = -\frac{k_B T}{e}\left(\frac{dV_{oc}}{dt}\right)^{-1} \quad (2)$$

The electron lifetime measurements are presented versus the solar cell's V_{oc} or the quasi-Fermi level of TiO_2.[4,8,14,30,33,34]

The In-TCPP(Sn) 60, 90, 120, and 150 μL cells had quick initial decay, while the 180 μL had a slower rate of decay as seen by the broader slope. Figure 4c additionally tracks the electron lifetime of the photogenerated species, and the negative slopes of T_n with increasing V_{oc} for the In-TCPP(Sn) cells is consistent with the electron lifetime decreasing at increasing quasi-Fermi levels.[30,33] The slope decay represents the electron charge transfer, as at increasing quasi-Fermi levels, the electron population in the TiO_2 layer is increased from excited charge injection. The longer decay period for the 180 μL cell was attributed to the slower electron injection into the TiO_2 valence band, causing the excited dye species to linger within the interfacial layers.[29] The Ti-TCPP and In-TCPP similarly demonstrated a slower voltage decay, with Ti-TCPP having a significantly slower decay. The slow voltage decay coupled with the sporadic line for the Ti-TCPP electron lifetime suggests the charge injection to the TiO_2 film was dramatically hampered. The slower voltage decay seen from the In-TCPP cell still retains a strong capability for charge injection, as the voltage decay and electron lifetime both depict steady slope decreases when not illuminated.

Section 3.5 – CV Scans of Ti-TCPP, In-TCPP, and In-TCPP (Sn)

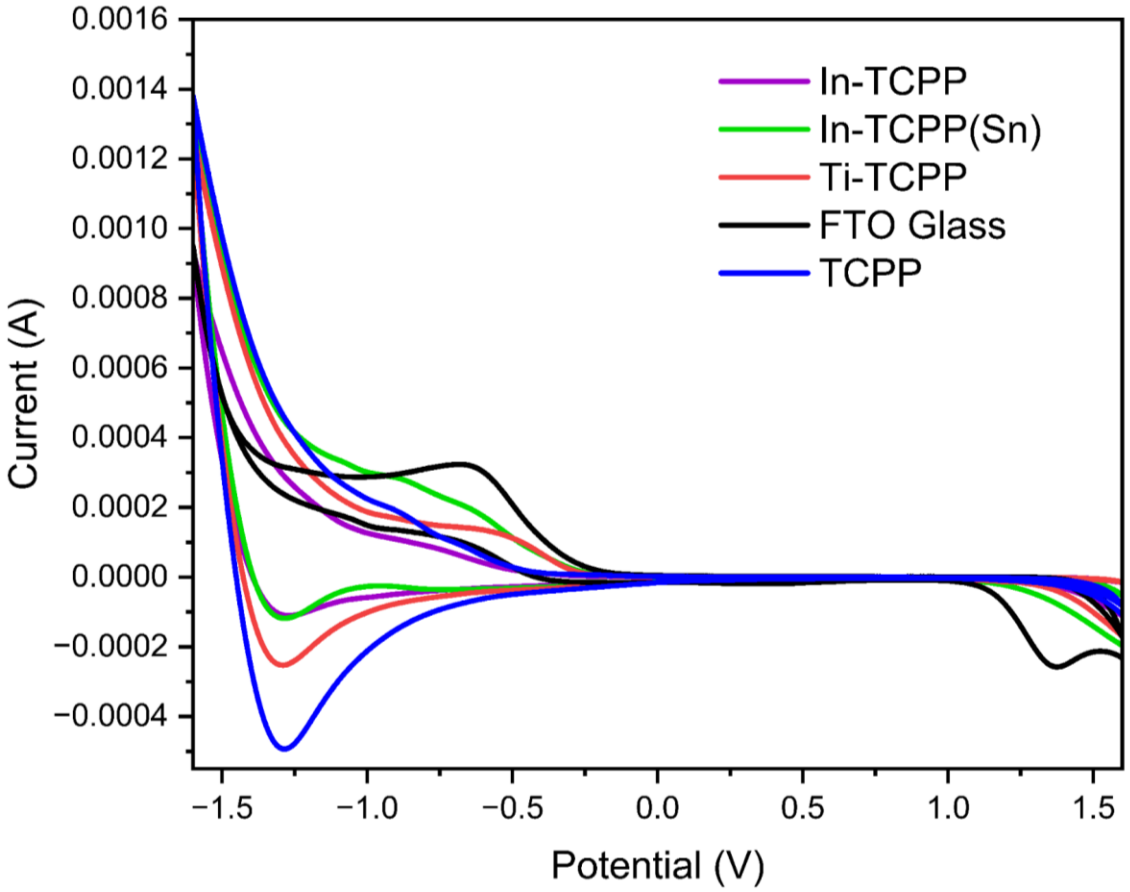

Figure 5. Cyclic voltammograms of Ti-TCPP, In-TCPP, and In-TCPP(Sn) MOF film cells compared against bare FTO glass.

To investigate the electrochemical capacitance of each MOF, the electrochemical measurements were taken in 1 M KCl electrolyte from -1.6 V to 1.6 V potential window. The CV scans were obtained, with Figure 5 depicting the oxidation and reductions MOF film cells. The bare FTO glass demonstrated a reduction peak at -0.65 V, indicating that the activity of hydrogen evolution and reduction of the tin-dopant, going from SnO_2 to Sn.[35] The anodic peak at 1.42 V was atrributed to the oxidation of the tin to tin oxide or oxyhydroxide. TCPP had redox couple peaks at -1.4V and at -0.8 V, deviating

significantly from the FTO glass. Ti-TCPP demonstrated a large shift in the peaks from the FTO glass, with a redox couple peak at -0.5 V and -1.3 V potentials. The peaks were attributed to possible redox activity coming from the π-conjugated system of the TCPP ligand, or the redox activity of the titanium cluster. In-TCPP and In-TCPP(Sn) demonstrate similar shifts in the peaks from the FTO glass scan, with both having sharp peak at -1.3 V and -0.8 V, with In-TCPP(Sn) seeing additional peaks at -0.4 V and -0.45 V. The peaks seen in In-TCPP were similarly attributed to the redox activity of the TCPP ligand, with the shift having deviated from the Ti-TCPP sample due to the indium cluster's influence. The In-TCPP(Sn) had two redox couple peaks, which could be due to the redox activity of the π-conjugated system in TCPP and the Sn(IV) in the porphyrin core experiencing a reduction.[16,35]

Conclusion

In summary, the Ti-TCPP, In-TCPP, and In-TCPP(Sn) were investigated for their use as photosensitizing dye of solid-state dye-sensitized solar cells. When the three MOF types were drop cast onto TiO_2 nanoparticle layers that were spin coated on the surface of FTO glass substrates, HTM and gold could be deposited to fabricate working ssDSSCs. The In-TCPP(Sn) 90 μL film cell exhibited the highest power conversion efficiency (η) value of 0.0243% with a high V_{oc} of 0.516 V, a drastic improvement from the cell fabricated with TCPP as the respective η and V_{oc} values were $6.35e^{-5}$% and 0.278 V. In-TCPP had comparable performance to the In-TCPP(Sn) cell, with a η of 0.0119% Ti-TCPP performed the worst of the three MOFs and the TCPP linker, having a lower efficiency of $2.25e^{-5}$%. The lifetime measurements determined that the electron injection using the MOFs were strong, as the π-conjugated system helped facilitate quick electron injection for In-TCPP and In-TCPP(Sn), whereas Ti-TCPP saw a suppressive effect on the electron injection to the TiO_2 layer that adversely affected its voltage decay. The cyclic voltammetry helped confirm the electrochemical activity of the three MOFs, with Ti-TCPP, In-TCPP, and In-TCPP(Sn) demonstrating redox couple activity. The potential of MOFs for enhancing ssDSSCs can be further studied, with future work potentially focusing on diversifying the MOF structures or incorporating different metals to investigate the effects on efficiency, charge transfer, and charge injection. Additionally, optimization of the cell fabrication process for ssDSSCs with higher layer uniformity can be done and extended to scalable fabrication methods for commercial applications. Lastly, a comprehensive stability test and environmental impact study can be done to

evaluate the sustainability of the fabricated photovoltaics, greatly improving the reach of practical applications.

REFERENCES

[1] B. K. Korir, J. K. Kibet, S. M. Ngari, *Energy Sci. Eng.* **2024**, *12*, 3188–3226.
[2] K. Abbass, M. Z. Qasim, H. Song, M. Murshed, H. Mahmood, I. Younis, *Environ. Sci. Pollut. Res.* **2022**, *29*, 42539–42559.
[3] H. Darmokoesoemo, H. Setyawati, I. Kris Murwani, M. Irfan, L. Adhitiya, A. Dania Audria Ulfa, R. Fuadi Prasetia, *Results Chem.* **2022**, *4*, 100646.
[4] S. Lin, T. Zhang, H. Yang, Y. Li, *Energy Fuels* **2024**, *38*, 761–788.
[5] A. Reale, L. Cinà, A. Malatesta, R. De Marco, T. M. Brown, A. Di Carlo, *Energy Technol.* **2014**, *2*, 531–541.
[6] J. A. Castillo-Robles, E. Rocha-Rangel, J. A. Ramírez-de-León, F. C. Caballero-Rico, E. N. Armendáriz-Mireles, *J. Compos. Sci.* **2021**, *5*, 288.
[7] B. O'Regan, M. Grätzel, *Nature* **1991**, *353*, 737–740.
[8] I. Benesperi, H. Michaels, M. Freitag, *J. Mater. Chem. C* **2018**, *6*, 11903–11942.
[9] X. Chen, S. S. Mao, *Chem. Rev.* **2007**, *107*, 2891–2959.
[10] A. A. Hendi, M. M. Alanazi, W. Alharbi, T. Ali, M. A. Awad, K. M. Ortashi, H. Aldosari, F. S. Alfaifi, R. Qindeel, G. Naz, T. H. Alsheddi, *J. King Saud Univ. - Sci.* **2023**, *35*, 102555.
[11] M. Sajid, G. Irum, A. Farhan, M. A. Qamar, *Hybrid Adv.* **2024**, *5*, 100167.
[12] B. Yadagiri, A. Kumar Kaliamurthy, K. Yoo, H. Cheol Kang, J. Ryu, F. Kwaku Asiam, J. Lee, *ChemistryOpen* **2023**, *12*, e202300170.
[13] S. Ramasamy, M. Bhagavathiachari, S. A. Suthanthiraraj, M. Pichai, *Dyes Pigments* **2022**, *203*, 110380.
[14] Ö. Birel, S. Nadeem, H. Duman, *J. Fluoresc.* **2017**, *27*, 1075–1085.
[15] J. M. D. Calmeiro, G. Gira, F. M. Ferraz, S. R. G. Fernandes, A. L. Pinto, L. M. O. Lourenço, J. P. C. Tomé, C. C. L. Pereira, *Dyes Pigments* **2020**, *177*, 108280.
[16] A. Rosa, G. Ricciardi, E. J. Baerends, A. Romeo, L. Monsù Scolaro, *J. Phys. Chem. A* **2003**, *107*, 11468–11482.
[17] S. Hiroto, Y. Miyake, H. Shinokubo, *Chem. Rev.* **2017**, *117*, 2910–3043.
[18] P. A. Angaridis, T. Lazarides, A. C. Coutsolelos, *Polyhedron* **2014**, *82*, 19–32.
[19] R. Ghamarpoor, A. Fallah, M. Jamshidi, *Sci. Rep.* **2023**, *13*, 9793.
[20] S. Gorjian, H. Ebadi, in *Photovolt. Sol. Energy Convers.*, Elsevier, **2020**, pp. 1–26.
[21] P. K. Goldberg, T. J. Pundsack, K. E. Splan, *J. Phys. Chem. A* **2011**, *115*, 10452–10460.
[22] A. B. Rudine, B. D. DelFatti, C. C. Wamser, *J. Org. Chem.* **2013**, *78*, 6040–6049.
[23] Y. Fang, P. Bhyrappa, Z. Ou, K. M. Kadish, *Chem. – Eur. J.* **2014**, *20*, 524–532.
[24] V. S. Chirvony, A. Van Hoek, V. A. Galievsky, I. V. Sazanovich, T. J. Schaafsma, D. Holten, *J. Phys. Chem. B* **2000**, *104*, 9909–9917.
[25] C. J. Kingsbury, K. J. Flanagan, H.-G. Eckhardt, M. Kielmann, M. O. Senge, *Molecules* **2020**, *25*, 3195.
[26] Y. Keum, S. Park, Y. Chen, J. Park, *Angew. Chem. Int. Ed.* **2018**, *57*, 14852–14856.
[27] T. Rhauderwiek, S. Waitschat, S. Wuttke, H. Reinsch, T. Bein, N. Stock, *Inorg. Chem.* **2016**, *55*, 5312–5319.
[28] N. K. Shee, H.-J. Kim, *Nanomaterials* **2025**, *15*, 59.
[29] X. Zou, R. B. Vadell, Y. Liu, A. Mendalz, M. Drillet, J. Sá, *J. Phys. Chem. C* **2022**, *126*, 21467–21475.

[30] C. Martín, M. Ziółek, A. Douhal, *J. Photochem. Photobiol. C Photochem. Rev.* **2016**, *26*, 1–30.
[31] M. N. Mustafa, Y. Sulaiman, *Sol. Energy* **2021**, *215*, 26–43.
[32] M. E. Hilal, A. Aboulouard, A. R. Akbar, H. A. Younus, N. Horzum, F. Verpoort, *Catalysts* **2020**, *10*, 897.
[33] A. R. Pascoe, F. Huang, N. W. Duffy, Y.-B. Cheng, *J. Phys. Chem. C* **2014**, *118*, 15154–15161.
[34] A. Zaban, M. Greenshtein, J. Bisquert, *ChemPhysChem* **2003**, *4*, 859–864.
[35] A. Korjenic, K. S. Raja, *J. Electrochem. Soc.* **2019**, *166*, C169–C184.